Prepared for submission to JHEP

Exploring the Higgs sector of the MRSSM with a light scalar

Philip Diessner,[a,1] **Jan Kalinowski,**[b] **Wojciech Kotlarski**[a,b] **and Dominik Stöckinger**[a]

[a] *Institut für Kern- und Teilchenphysik, TU Dresden*
01069 Dresden, Germany
[b] *Faculty of Physics, University of Warsaw,*
Pasteura 5, 02093 Warsaw, Poland

E-mail: philip.diessner@mailbox.tu-dresden.de,
jan.kalinowski@fuw.edu.pl, wojciech.kotlarski@fuw.edu.pl,
dominik.stoeckinger@tu-dresden.de

Abstract: In a recent paper we showed that the Minimal R-symmetric Supersymmetric Standard Model (MRSSM) can accommodate the observed 125 GeV Higgs boson as the lightest scalar of the model in agreement with electroweak precision observables, in particular with the W boson mass and T parameter. Here we explore a scenario with the light singlet (and bino-singlino) state in which the second-lightest scalar takes the role of the SM-like boson with mass close to 125 GeV. In such a case the second-lightest Higgs state gets pushed up via mixing already at tree-level and thereby reducing the required loop correction. Unlike in the NMSSM, the light singlet is necessarily connected with a light neutralino which naturally appears as a promising dark matter candidate. We show that dark matter and LHC searches place further bounds on this scenario and point out parameter regions, which are viable and of interest for LHC Run II and upcoming dark matter experiments.

[1] Corresponding author.

arXiv:1511.09334v2 [hep-ph] 10 Dec 2015

Contents

1 Introduction **2**

2 Higgs constraints **4**
- 2.1 Scenario description 4
- 2.2 Quantitative analysis and comparison to experiment 6

3 LHC constraints **10**
- 3.1 Constraints from slepton searches 10
- 3.2 Qualitative description of the MRSSM chargino/neutralino sector 11
- 3.3 Setup for recasting LHC limits for the MRSSM 12
- 3.4 Light staus and light charginos 14
- 3.5 General investigation of light charginos 15

4 Dark matter constraints **17**
- 4.1 Relic density 18
- 4.2 Direct detection 19

5 Summary and conclusions **22**

A MRSSM mass matrices at tree level **25**

1 Introduction

After the discovery of a Standard Model (SM)-like Higgs boson at the LHC [1–3], it remains an open question whether there are additional scalar particles, possibly even with smaller mass. Supersymmetric models always predict the existence of additional scalars, and the possibility of light scalars has been explored both in the minimal supersymmetric standard model (MSSM) [4–6] and in its extensions, such as the NMSSM which contains a gauge singlet field [7, 8]. In the NMSSM a light singlet-like scalar is motivated since it pushes the tree-level value of the SM-like Higgs boson mass up towards the observed value, reducing the need for large loop corrections [9–21]. The interplay of the Higgs sector and dark matter results in the MSSM and NMSSM was further discussed in [22–28].

In the present paper we consider the possibility of a light, singlet-like scalar in the minimal R-symmetric supersymmetric model, the MRSSM [29]. We show that it is necessarily connected with a very light neutralino LSP, and we explore the phenomenology of the Higgs sector and the related chargino/neutralino sector, taking into account collider and dark matter constraints.

The MRSSM is quite distinct from the usual MSSM and NMSSM and is motivated in several ways. Its essential feature is an exact, global U(1) R-symmetry [30, 31], under which SM-fields and superpartners have different charges. This symmetry is stronger than R-parity, and it forbids Majorana masses for gauginos, the MSSM Higgsino mass parameter μ, and all left-right sfermion mixings. As a result, several of the most important experimental constraints on supersymmetry are alleviated: contributions to CP- and flavour-violating observables are suppressed even in presence of flavour violation in the sfermion sector [29, 32], and the production cross section for squarks is reduced, making squarks below the TeV scale generically compatible with LHC data [33].

The most exciting implication of R-symmetry from the point of view of scalars is that additional scalar fields are not ad hoc but are enforced by an N=2 supersymmetric structure of the gauge/gaugino sector: for each gauge group factor, there are gauge fields, Dirac instead of Majorana gauginos, and scalar fields in the adjoint representation. The MRSSM therefore contains sgluons – colour-octet scalars, a scalar SU(2) triplet, and a scalar singlet. This scalar singlet behaves quite differently and is more strongly connected to the other sectors of the theory than the singlet of the NMSSM.

Previous phenomenological investigations of the MRSSM have not focused on a light singlet, but it has been shown that models with R-symmetry and/or Dirac gauginos contain promising dark matter candidates [34–36], and the collider physics of the extra, non-MSSM-like states has been studied [37–45].

Recently in Refs. [46, 47] the lightest (SM-like) Higgs boson mass has been computed at the one-loop and leading two-loop level and the W-boson mass has been computed taking into account tree-level corrections to ρ from the triplet vacuum expectation value and full one-loop corrections to muon decay. It was shown that the measured value of the Higgs boson mass at the LHC can be accommodated in the MRSSM even for top squarks as light as 1 TeV. The outcome of these calculations was not obvious since in the MRSSM the lightest Higgs boson tree-level mass is typically reduced compared to the MSSM due

	BMP4	BMP5	BMP6
$\tan\beta$	40	20	6
B_μ	200^2	200^2	500^2
λ_d, λ_u	$0.01, -0.01$	$0.0, -0.01$	$0.0, 0.0$
Λ_d, Λ_u	$-1, -1.2$	$-1, -1.15$	$-1, -1.2$
M_B^D	50	44	30
m_S^2	30^2	40^2	80^2
$m_{R_u}^2$, $m_{R_d}^2$		$1000^2, 700^2$	
μ_d, μ_u	$130, 650$	$400, 550$	$550, 550$
M_W^D	600	500	400
M_O^D		1500	
m_T^2, m_O^2		$3000^2, 1000^2$	
$m_{Q;1,2}^2$, $m_{Q;3}^2$	$1500^2, 700^2$	$1300^2, 700^2$	$1400^2, 700^2$
$m_{D;1,2}^2$, $m_{D;3}^2$	$1500^2, 1000^2$	$1300^2, 1000^2$	$1400^2, 1000^2$
$m_{U;1,2}^2$, $m_{U;3}^2$	$1500^2, 700^2$	$1300^2, 700^2$	$1400^2, 700^2$
$m_{L;1,2}^2$, $m_{E;1,2}^2$	800^2, 800^2	1000^2, 1000^2	500^2, 350^2
$m_{L;3,3}^2$, $m_{E;3,3}^2$	800^2, 136^2	1000^2, 1000^2	500^2, 95^2
m_{H_d}	1217^2	211^2	1042^2
m_{H_u}	$-(767^2)$	$-(207^2)$	$-(201)^2$
v_S	-64.9	-42.5	-56.1
v_T	-1.08	-1.2	-1.1

Table 1. Benchmark points for the scenario discussed here. Dimensionful parameters are given in GeV or GeV^2, as appropriate.

to mixing with the additional scalars, and the loop corrections cannot be enhanced by stop mixing. However, the new fields and couplings can give rise to the necessary large loop contributions to the Higgs mass without generating too large a contribution to the W-boson mass. For a similar analysis see Ref. [48], where also a welcome reduction of the level of fine-tuning was found.

The plan of the present paper is as follows. In section 2 we remind the reader on the relevant model details and will describe how demanding a light singlet scalar constrains the parameter space of the model. Sections 3 and 4 study how LHC and dark matter bounds, respectively, are affected by these constraints. To highlight features of different regions of parameters, which are also in agreement with LHC and dark matter searches, we define the new Benchmark points given in Tab. 1. They feature many states well below 1 TeV, including the top squark masses. The combination of all different experimental constraints on the parameter space of the MRSSM is summarized in section 5 which also contains our conclusions.

2 Higgs constraints

2.1 Scenario description

The essential field content and parameters of the MRSSM can be read off from the superpotential

$$\begin{aligned} W =& \mu_d \hat{R}_d \cdot \hat{H}_d + \mu_u \hat{R}_u \cdot \hat{H}_u + \Lambda_d \hat{R}_d \cdot \hat{T} \hat{H}_d + \Lambda_u \hat{R}_u \cdot \hat{T} \hat{H}_u \\ &+ \lambda_d \hat{S} \hat{R}_d \cdot \hat{H}_d + \lambda_u \hat{S} \hat{R}_u \cdot \hat{H}_u - Y_d \hat{d} \hat{q} \cdot \hat{H}_d - Y_e \hat{e} \hat{l} \cdot \hat{H}_d + Y_u \hat{u} \hat{q} \cdot \hat{H}_u \,. \end{aligned} \tag{2.1}$$

The MSSM-like fields are the Higgs doublet superfields $\hat{H}_{d,u}$ and the quark and lepton superfields $\hat{q}$, $\hat{u}$, $\hat{d}$, $\hat{l}$, $\hat{e}$. The Yukawa couplings are the same as in the MSSM. The new fields are the doublets $\hat{R}_{d,u}$, which contain the Dirac mass partners of the higgsinos and the corresponding Dirac higgsino mass parameters are denoted as $\mu_{d,u}$. The singlet, the SU(2)-triplet and the color-octet chiral superfields, $\hat{S}$, $\hat{T}$ and $\hat{O}$, contain the Dirac mass partners of the usual gauginos. The superpotential contains Yukawa-like trilinear terms involving the new fields; the associated parameters are denoted as $\lambda_{d,u}$ for the terms involving the singlet and $\Lambda_{d,u}$ for the terms involving the triplet; terms involving the octet are not allowed by R-symmetry. Further important parameters of the MRSSM are the Dirac mass parameters $M^D_{B,W,O}$ for the U(1), $\mathrm{SU}(2)_L$ and $\mathrm{SU}(3)_c$ gauginos, respectively, the soft scalar mass parameters $m^2_{S,T,O}$ for the singlet, triplet and octet states, the soft mass parameters $m^2_{H_d,H_u,R_d,R_u}$ for the Higgs and R-Higgs bosons, and the standard B_μ parameter and sfermion mass parameters, while the trilinear sfermion couplings are forbidden by R-symmetry. The explicit form of the soft SUSY breaking potential is given in Ref. [46].

We begin the discussion with the neutral Higgs sector of the MRSSM. There are four complex (electrically and R-charge) neutral scalar fields, which can mix. Their real and imaginary parts, denoted as $(\phi_d, \phi_u, \phi_S, \phi_T)$ and $(\sigma_d, \sigma_u, \sigma_S, \sigma_T)$, correspond to the two MSSM-like Higgs doublets $H_{d,u}$, and the $N = 2$ scalar superpartners of the hypercharge and $\mathrm{SU}(2)_L$ gauge fields, S and T. Since their vacuum expectation values, denoted as $v_{d,u,S,T}$ respectively, are assumed real, the real and imaginary components do not mix, and the mass-square matrix breaks into two 4x4 sub-matrices.

In the pseudo-scalar sector the MSSM-like states (σ_d, σ_u) do not mix with the singlet-triplet states (σ_S, σ_T) and the mass-square matrix breaks further into two 2x2 sub-matrices, see Appendix A. Therefore the neutral Goldstone boson and one of the pseudo-scalar Higgs bosons A with $m_A^2 = 2B_\mu / \sin 2\beta$ appear as in the MSSM. On the other hand, in the (σ_S, σ_T) sector the mixing is negligible for a heavy triplet mass m_T and the lightest pseudo-scalar state is almost a pure singlet with its mass given by the soft parameter m_S. Therefore, to a good approximation it decouples and is of no interest for the following discussion.

In the scalar sector all fields mix and the full 4x4 tree-level mass-square matrix $\mathcal{M}^\phi$ in the weak basis $(\phi_d, \phi_u, \phi_S, \phi_T)$ has been given explicitly in Ref. [46]. It is diagonalized by a unitary rotation $Z^H \mathcal{M}^\phi Z^{H\dagger}$ to the mass-eigenstate basis (H_1, H_2, H_3, H_4), ordered with increasing mass. For the qualitative discussion we consider the limit in which the triplet decouples due to a high soft breaking mass term m_T (a necessary condition to suppress the tree-level triplet contribution to the W boson mass and ρ parameter), and in which the

pseudoscalar Higgs mass M_A and the value of $\tan\beta = v_u/v_d$ become large. In this limit the SM-like Higgs boson is dominantly given by the up-type field ϕ_u, and to highlight the main effect of the mixing in the light-scalar scenario it is enough to recall the most relevant part of the mass-square matrix, namely the 2x2 sub-matrix corresponding to the (ϕ_u, ϕ_S) fields only, which reads

$$\mathcal{M}^{\phi}_{u,S} = \begin{pmatrix} m_Z^2 + \Delta m^2_{rad} & v_u\left(\sqrt{2}\lambda_u \mu_u^{\text{eff},-} + g_1 M_B^D\right) \\ v_u\left(\sqrt{2}\lambda_u \mu_u^{\text{eff},-} + g_1 M_B^D\right) & 4(M_B^D)^2 + m_S^2 + \frac{\lambda_u^2 v_u^2}{2} \end{pmatrix} , \tag{2.2}$$

where we have included the dominant radiative correction Δm^2_{rad} to the diagonal element of the doublet field ϕ_u, and we have used the abbreviations

$$\mu_i^{\text{eff},\pm} = \mu_i + \frac{\lambda_i v_S}{\sqrt{2}} \pm \frac{\Lambda_i v_T}{2}, \qquad\qquad i = u, d. \tag{2.3}$$

The parameters M_B^D, μ_u and λ_u appear in the scalar potential due to supersymmetry.[1] From this approximation to the mass-square matrix we can draw several immediate consequences on the four most important parameters in the light-singlet scenario in which $m_{H_1} < m_{H_2} \approx 125$ GeV.

a) Singlet soft mass m_S^2:

The soft breaking parameter m_S^2 appears in the diagonal element for the singlet field ϕ_S in the mass matrix (2.2). To ensure that the lightest scalar state is a singlet-like a direct upper limit can be put on this parameter:

$$m_S^2 < m_Z^2 + \Delta m^2_{rad} \, , \tag{2.4}$$

Therefore the numerical value of m_S^2 has to be limited to be below $\approx (120 \text{ GeV})^2$

b) Dirac bino-singlino mass M_B^D:

Due to supersymmetry, the Dirac mass parameter M_B^D appears also in the singlet diagonal element, and moreover in the off-diagonal elements as well. Hence, a direct upper limit can be derived

$$(M_B^D)^2 < \frac{m_Z^2 + \Delta m^2_{rad}}{4} \approx (60 \text{ GeV})^2 \, , \tag{2.5}$$

similar to the one on m_S^2 (however stronger) to keep the singlet-diagonal element smaller than the doublet one. Of course, the bino-singlino mass parameter appears also in the neutralino mass matrix and is the dominant parameter that determines the LSP mass in the light singlet/bino-singlino scenario. Therefore constraints from dark matter and direct LHC searches for neutralinos will have a strong impact on the Higgs sector.

c) Higgsino mass μ_u:

The higgsino mass parameter μ_u appears in the off-diagonal element of the mass matrix in Eq. (2.2) in combination with λ_u. However μ_u also enters as a parameter in the

[1] In Ref [49] it was recently shown that Dirac masses could also be generated without contributions to the scalar sector. Here, we keep with the usual D-term generation of these mass terms for the MRSSM.

chargino/neutralino sector, and it is strongly limited from below by the direct chargino searches and dark matter constraints. We recall that μ_u has a strong influence on the loop corrections Δm^2_{rad} to the doublet component ϕ_u, so it can affect the mixing additionally through that diagonal element.

d) Yukawa-like parameter λ_u:

The Yukawa-like parameter λ_u multiplies the higgsino mass parameter μ_u in the off-diagonal element of Eq. (2.2). The off-diagonal element cannot be too large in order to avoid a negative determinant of the mass matrix and thus tachyonic states. In the simple limit $v_S, m_Z \ll \mu_u$, avoiding tachyons leads to the following bound on λ_u:

$$\left|\lambda_u + \frac{g_1 M_B^D v_u}{\sqrt{2}\mu_u v_u}\right| < \frac{m_Z\sqrt{4(M_B^D)^2 + m_S^2}}{\sqrt{2}\mu_u v_u} \tag{2.6}$$

There can be a cancellation between λ_u and the M_B^D-term, but since μ_u is much larger than all other appearing mass parameters, the value of λ_u is necessarily very small.

In summary, these simple considerations lead to the following promising parameter hierarchies for a light singlet scenario:

$$m_S, M_B^D \quad < \quad m_Z \quad < \quad \mu_u\,, \qquad\qquad |\lambda_u| \quad \ll \quad 1\,. \tag{2.7}$$

2.2 Quantitative analysis and comparison to experiment

In our phenomenological investigations we will of course not use the approximations made before but we will always use the most precise available expressions including higher order corrections. This is done using the *Mathematica* [50] package `SARAH` [51–56] and `SPheno` [57, 58]. This approach was cross-checked, as described in Refs. [46, 47], using `FlexibleSUSY`[59], `FeynArts` and `FormCalc` [62–64].

Fig. 1 shows a quantitative analysis of the mixing of the two lightest Higgs states, as a function of the two relevant parameters m_S (left column) and M_B^D (right column). The other parameters are chosen as in BMP5, given in Tab. 1. They satisfy the hierarchy of Eq. (2.7); the precise parameter choices will be motivated in the subsequent sections.

The first two lines in the figure show the masses of the two lightest Higgs states (computed to two-loops as described in Ref. [47]) and the singlet component of these two states, measured by the square of the corresponding mixing matrix elements $(Z^H_{H_1,\phi_S})^2$ and $(Z^H_{H_2,\phi_S})^2$. As expected from the discussion above, as long as the approximate inequalities Eq. (2.4) and Eq. (2.5) are satisfied, the lightest state is significantly lighter than m_Z and has a high singlet component. Once m_S or M_B^D become heavier, the lightest state becomes mainly a doublet-like (and hence SM-like) and its mass approaches a limit, which is here below 120 GeV. Which of the parameter regions is phenomenologically viable will be determined below.

The third line of plots in Fig. 1 quantifies one of the major motivations for the light singlet scenario — the enhancement of the SM-like Higgs boson mass due to the tree-level push resulting from mixing with the scalar state. The plots show the difference of the actual value of this mass and the value in a reference case, in which all Higgs bosons except the

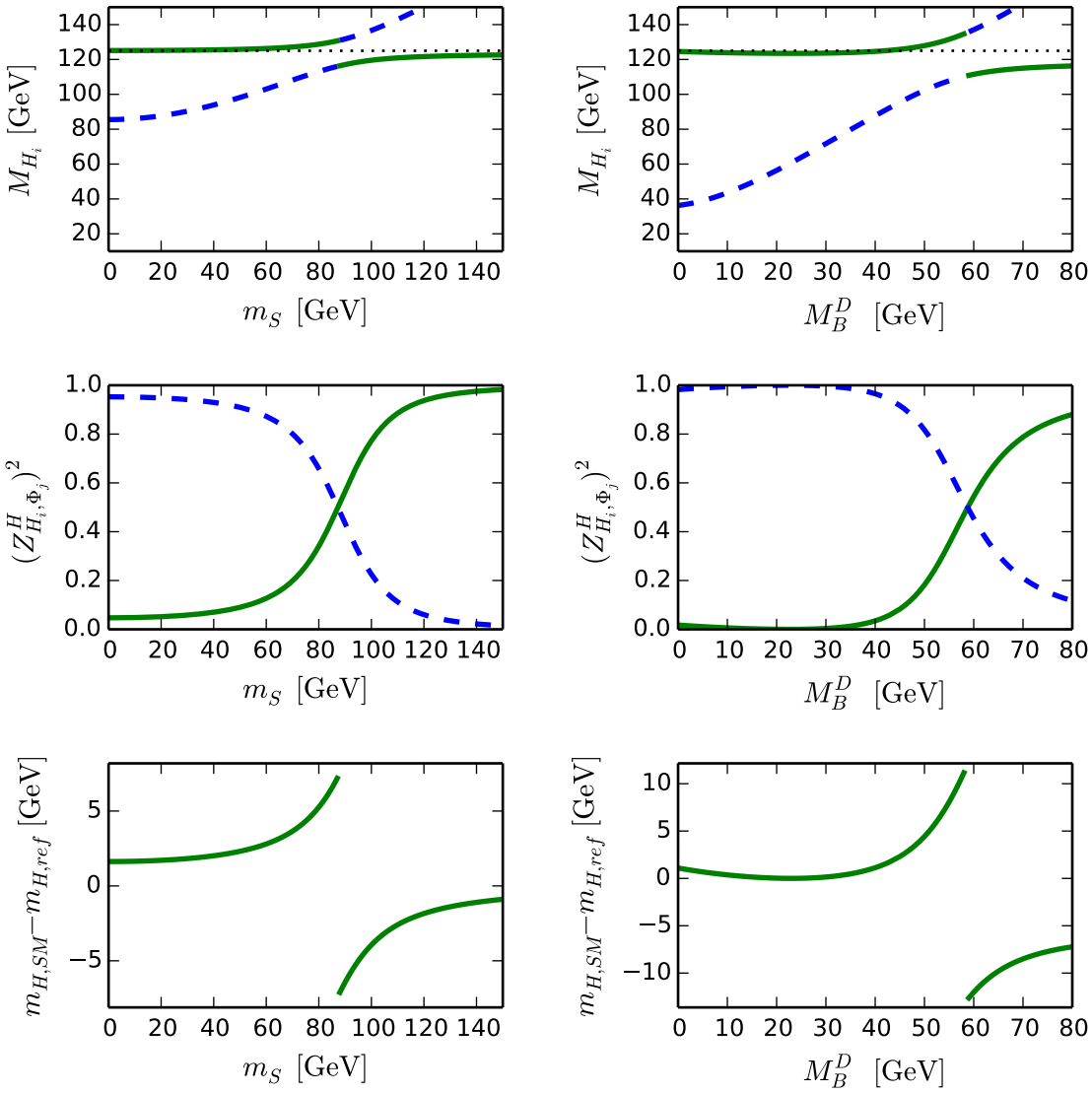

Figure 1. Level crossing of lightest and second-lightest Higgs state for BMP5, depending on the dimensionful parameter m_S (M_B^D) on the left (right). Top row shows the masses of the lightest and second-lightest mass eigenstate, the green full line is more SM-like, while the blue dashed line is singlet-like.The second line shows the mixing parameter as described in the text. The blue dashed line is the singlet content of the lightest mass eigenstate, the green full line the doublet content. The bottom row gives the relative mass shift compared to a reference mass, where the mixing between singlet and doublet vanishes.

SM-like one are very heavy. In the light-singlet case, the upward shift can amount to more than 10 GeV. The upward shift is particularly strong for non-vanishing Dirac mass M_B^D, since this parameter also appears in the off-diagonal element of the mass matrix Eq. (2.2).

Now we compare the light-singlet scenario illustrated in Fig. 1 with experimental data.

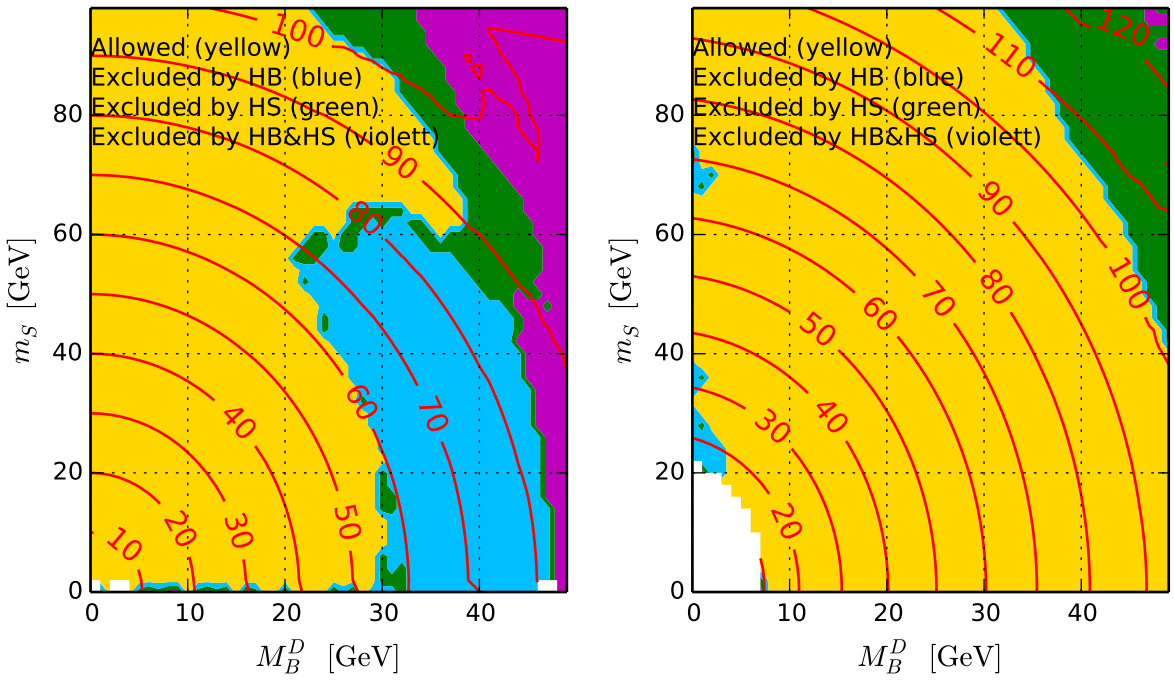

Figure 2. Exclusion plot using `HiggsSignals-1.3` and `HiggsBounds-4.2`; Higgs masses are calculated at two loops. Scanned over Λ_u and projected onto the plane. If there is one Λ_u for a point giving non-exclusion, it is shown as non-excluded. Scanning from $-1.5 < \Lambda_u < 0$, while $\lambda_u = 0/-0.01$ (left,right). Red contours show the lightest Higgs boson mass.

It is clear that there are two kinds of direct constraints on the two lightest scalars and their mixing. On the one hand, there must be a SM-like state which can be identified with the Higgs boson observed at LHC, with mass compatible with the observed value and with sufficiently small singlet mix-in in order to agree with the observed Higgs signal strengths and branching ratios. On the other hand, the state that is lighter than the one observed at the LHC must be sufficiently singlet-like in order to evade limits from direct searches for light scalars, especially the LEP searches. Roughly speaking, for light singlet masses these constraints restrict the mixing to around $(Z^H_{H_1,\phi_u})^2 < 0.02$, except for the region, where LEP saw an upward fluctuation. Here the mixing is restrained to $(Z^H_{H_1,\phi_u})^2 < 0.15$.

Both types of constraints can be precisely analyzed with the help of `HiggsBounds`-4.2 and `HiggsSignals`-1.4, respectively [65–70]. Here, we pass the effective couplings written by `SPheno` to both tools for each parameter point studied. With `HiggsBounds` the option *LandH* is used to check the MRSSM Higgs sector against all experimental constraints included with the program. For `HiggsSignals` all peak observables available are used (option *latestresults* and *peak*), the mass uncertainties are described using a Gaussian shape and we estimate the uncertainty of the SM-like Higgs boson mass with 3 GeV.

The interpretation of the `HiggsBounds` and `HiggsSignals` results is done in a simplified way. A parameter point is excluded by `HiggsBounds` by using the 95% CL limit of its

	BMP4	BMP5	BMP6
m_{H_1}	100	94	95
m_{H_2}	125.8	125.5	125.8
`HiggsSignals` p-value	0.75	0.76	0.72
Allowed by `HiggsBounds`	✓	✓	✓
m_W	80.384	80.392	80.404

Table 2. Higgs sector observables: masses of the Higgs bosons, `HiggsSignals` p-value, `HiggsBounds` check and, for completeness, the W boson mass for the benchmark points. Dimensionful parameters are given in GeV.

output and by `HiggsSignals` when its approximately calculated p-value is smaller than 0.05. A point is excluded by both when both constraints apply. For a more complete statistical treatment of extended Higgs sectors containing light singlet scenarios for the singlet-extended SM and NMSSM see Refs. [71] and [72], respectively. In the case of the MRSSM this approach is left for future work.

Fig. 2 shows the resulting excluded and allowed regions in the plane of m_S and M_B^D for two different values of λ_u. The parameter Λ_u is adjusted to ensure the correct mass of the observed Higgs boson; the remaining parameters are fixed as in BMP5. The combination of the two plots shows that complete range of m_S and M_B^D discussed before with simple approximations of the tree-level scalar mass matrix is viable, except of the region of level crossing and very strong mixing. We find that the light-singlet scenario can be realized in the MRSSM for $m_S < 100$ GeV and $M_B^D < 55$ GeV. However, the two plots also show very high sensitivity to the small λ_u, which appears essentially in combination with the very small term $\propto M_B^D/\mu_u$, see (2.6). Changing it from zero to (-0.01) leads to strong shifts of the allowed regions.

The main novel feature of the light-singlet scenario in the MRSSM is the restriction on the Dirac bino-singlino mass M_B^D. This restriction has no counterpart e.g. in the NMSSM. Obviously this limit affects the neutralino sector. Combined with LEP bounds on chargino and neutralino production it leads to the conclusion that the LSP is a Dirac bino-singlino neutralino with mass related to M_B^D and thus limited from above. This limit on the LSP mass will provide strong constraints from and correlations to LHC processes and dark matter studies.

With these restrictions on m_S and M_B^D, the decay of the Z and SM-like Higgs boson into the LSP and singlet-like Higgs boson, if kinematically allowed, needs to be sufficiently suppressed so that theoretical prediction of invisible width of both particles is in agreement with experiment. In the mass region of interest, $m_{H_1} < 62$ GeV, `HiggsBounds` puts very stringent limits on the singlet-doublet mixing. As the decay of the SM-like Higgs boson into the light (pseudo-)scalar is related to this mixing, contributions of these decay channels are strongly reduced for realistic scenarios. Decays of Z (Higgs) bosons to LSPs are induced by the couplings to the (R-)higgsino (higgsino+bino or R-higgsino+singlino) parts of the

LSP. This is mainly mediated by gauge couplings and will be suppressed by the weak (R-)higgsino–singlino-bino–mixing. We will show that it is also important for direct detection limits from dark matter searches. These searches put such a strong bound on the mixing so that the decay to the LSP will be automatically suppressed.

Table 2 summarizes the Higgs sector observables for our benchmark points, as well as the predicted W boson mass.

3 LHC constraints

As was discussed in the previous section, demanding the singlet state to give the lightest Higgs boson yields a direct upper limit on the Dirac bino mass M_B^D. A light bino-like neutralino, and more generally light weakly interacting particles, are promising in two respects. They might lead to observable signals at the LHC, and they might explain the observed dark matter relic density. At the same time, the light-singlet scenario is constrained by existing data from LHC and dark matter searches. In the present section we study the constraints from LHC in detail. We only consider constraints on weakly interacting particles, i.e. on charginos, neutralinos, and sleptons. All strongly interacting particles are not relevant for the electroweak and dark matter phenomenology studied here and are assumed to be heavy enough to evade limits.

So far the negative results of LHC searches for new particles have been interpreted within the MSSM, or a number of simplified models which include a pair of charginos, the neutralinos and gluinos are of the Majorana type, and left- and right-chiral sfermions that can mix. In general, care has to be taken in reinterpreting the LHC bounds in the context of the MRSSM, since the MRSSM differs from the MSSM in the number of degrees of freedom, the Dirac versus Majorana nature of neutralinos, the mixing patterns, and since some processes are forbidden in the MRSSM due to the conserved R-charge.

3.1 Constraints from slepton searches

We first discuss briefly the simplest case of constraints following from slepton searches. In both the MSSM and the MRSSM, sleptons can be produced in pairs through Drell-Yan processes. In the MRSSM, slepton left-right mixing vanishes, which is not an essential difference to the MSSM, where the mixing is typically assumed to be small. In both models, light sleptons will decay directly to the corresponding leptons and the bino-like neutralino LSP. In such a case the Dirac or Majorana nature of the LSP does not matter and, hence, the MSSM exclusion bounds for light sleptons can be applied directly to the MRSSM case. Recently the ATLAS Collaboration derived the exclusion limits in the $(m_{\tilde{\ell}_{L,R}}, m_{\tilde{\chi}_1^0})$ parameter space from the analyses of the selectron and smuon pair-production processes, see Figs. 8 (a) and (b) of Ref. [73].[2] These exclusion limits can be specialized to our case, in which Eq. (2.5) implies an upper limit of ≈ 55 GeV on the LSP mass. We then find that left-handed slepton masses below ≈ 300 GeV are excluded. For the right-handed slepton masses the bound is somewhat weaker (around 250 GeV) due to smaller production cross

[2]Similar limits are also given by the CMS collaboration [74].

section. Further, a small corner at a lower right-handed slepton mass ~ 100 GeV with the LSP masses in the range 40-55 GeV is still allowed. With the current experimental reach the direct production of staus with the cross sections predicted by supersymmetry can not be excluded, see Ref. [75].

The remainder of the present section is devoted to the more interesting case of neutralino and chargino searches.

3.2 Qualitative description of the MRSSM chargino/neutralino sector

The chargino and neutralino sectors of the MSSM and the MRSSM are quite different. In the MRSSM, the neutralinos are Dirac fermions composed of eight Weyl spinors $\xi_i = (\tilde{B}, \tilde{W}^0, \tilde{R}_d^0, \tilde{R}_u^0)$ and $\zeta_i = (\tilde{S}, \tilde{T}^0, \tilde{H}_d^0, \tilde{H}_u^0)$. The four mass eigenvalues are dominantly given by the four independent mass parameters $(M_B^D, M_W^D, \mu_d, \mu_u)$, see Appendix A. In contrast, in the MSSM the neutralinos are Majorana fermions, and there is only a single higgsino mass parameter μ, so that two neutralino masses are approximately degenerate.

The MRSSM comprises four different charginos, with masses determined by the wino and the two higgsino mass parameters, see Appendix A. In contrast, the MSSM contains only two charginos.

Table 3 gives an overview of possible observed signatures of sets of charginos and neutralinos (listed in the first column). It then shows the corresponding possible interpretations of the signatures in the MSSM (second column) and in the MRSSM (third column), which are very different as can be understood on the basis of the previous remarks. The table is more general than necessary for the purposes of the present paper, and it can serve as a basis of further investigations of the LHC phenomenology of the MRSSM.

In general, as the number of degrees of freedom for neutralinos and charginos is twice as large in the MRSSM than in the MSSM one could naively expect an enhancement of the production cross section by a factor of four. However, all MRSSM charginos and neutralinos carry non-vanishing R-charge. Due to R-charge conservation, therefore, only half of all final state combinations is allowed. Furthermore, the new genuine MRSSM states $(\tilde{R}_d, \tilde{R}_u, \tilde{S}, \tilde{T})$ do not interact at tree level with fermions, sfermions or gluons. Hence the situation is more complicated and has to be analyzed channel by channel.

Further differences between MRSSM and MSSM exist in the couplings of charginos and neutralinos and therefore in the decay branching ratios. For example, in the MSSM the higgsino mass parameter μ induces a maximal mixing between the up- and down-higgsino so that both will mix almost similarly with the bino and wino, implying an appreciable decay rates of both higgsinos to sleptons, if kinematically available. This is different in the MRSSM. R-symmetry does not allow a parameter which induces mixing between the up- and down-(R-)higgsinos, instead separate mass parameters μ_d and μ_u are needed. Then, up- and down-(R-)higgsino states separately will be good approximations to the corresponding mass eigenstates. For $\tan\beta \gg 1$ this also means that the mixing between down-(R-)higgsino with the wino-triplino and bino-singlino states will be strongly suppressed. As a result, for large $\tan\beta$ the down-(R-)higgsino has appreciable couplings only to staus, which are not shared with the up-(R-)higgsino.

experimental signature	**MSSM**	**MRSSM**
1 charged and 1 neutral of similar mass	wino-like states	either up- or down-(R-)higgsino-like states
2 charged and 1 neutral of similar mass	-	wino-triplino-like states
1 charged and 2 neutral of similar mass	higgsino-like states	-
2 charged and 2 neutral of similar mass	-	either up- or down-(R-)higgsino-like states
2 charged and 3 neutral of similar mass	all states	-
3 charged and 2 neutral of similar mass	-	wino-triplino-like and either up- or down-(R-)higgsino-like states
4 charged and 3 neutral of similar mass	-	all states

Table 3. Possible discovery scenarios at colliders of different sets of particles from the neutralino-chargino sector and the corresponding dominant gauge eigenstates for the MSSM and MRSSM. This is assuming the light-singlet-scenario in the MRSSM, which leads to a light bino-singlino as LSP candidate.

It is also important to consider decays of charginos and neutralinos into the SM-like Higgs boson H_2 observed at the LHC or into the light singlet H_1, present in our scenario. These decays are influenced by the λ/Λ parameters. Large Λ are needed to generate large enough loop contributions to the mass of the SM-like Higgs boson and λ needs to be small in the light singlet scenario studied here. Therefore, the decay of the wino-triplino to the SM-like Higgs boson and LSP, if kinematically allowed, will be enhanced by Λ, while contributions from λ to the higgsinos decaying to the SM-like Higgs boson and LSP are small.

When the chargino/neutralino decay to the SM-like Higgs boson is kinematically not possible, decays to the light singlet in our scenario still might open. Therefore, it can be a competing channel to the decay to the Z boson above the Z boson mass or the dominant decay channel below it. For higher neutralino masses the branching ratio to the light singlet will be sub-dominant to the one to the SM-like Higgs boson, but might still be non-negligible, depending on the mixing between singlet and doublets.

3.3 Setup for recasting LHC limits for the MRSSM

After having given an overview on the qualitative details of electro-weak production in the MRSSM, we now turn to a more in-depth analysis, taking the experimental input into account in a systematic way.

process	$\chi^0\bar{\chi}^0$	$\chi^0\chi^-$	$\chi^0\rho^+$	$\chi^+\bar{\chi}^0$	$\rho^-\bar{\chi}^0$	$\chi^+\chi^-$	$\rho^+\rho^-$	$\tilde{\ell}^+_{R,i}\tilde{\ell}^-_{R,j}$
BMP4	496	619	3.9	1147	0.83	496	1.25	17.6
BMP5	4.77	5.58	10.0	15.6	1.99	7.93	2.88	1.48×10^{-3}
BMP6	1.67	6.04	22.6	17.0	5.65	12.1	8.48	38.4

Table 4. EW cross sections as calculated by `Herwig++` using the `SARAH` model input. All values given in fb.

In recent years different computational tools emerged, which try to automatize the study of beyond the Standard Model physics at the LHC in a rather generic way using standardized interfaces. This allows us to take the model differences between the MRSSM and the MSSM/simplified models studied by the experiments into account and directly calculate bounds from the LHC on the MRSSM parameter space. In the following, we give a description of the set of tools used to for this.

Using the `UFO` [76] output produced by `SARAH` with `Herwig++`-2.7 [77, 78][3] we simulate the LO production of electro-weak sparticles at the LHC and compare it with 8 TeV data with `CheckMATE`-1.2.0 [81].[4] `CheckMATE` includes ATLAS analyses, which can be sensitive to the final state of these processes, when several leptons appear as decay products. Specifically, we take into account the analyses implemented in `CheckMATE` for two [73, 87], three [88, 89] and four and more leptons [90] in the final state. The final output of `CheckMATE` used to set exclusion limits in the MRSSM parameter space is the value for CL_S of most sensitive signal region of the studied analyses for each parameter point.

To ensure correctness of the calculated limits several tests of the used tools were done. For the calculation of the matrix element the event generator `Herwig++`-2.7 was checked against `Madgraph 5` [91], `FeynArts`/`FormCalc` and `CalcHEP` [92], where also the input of the model files was produced by `SARAH`. Agreement was achieved up to the implementation differences of the programs. The analyses implementation by `CheckMATE` was checked by recalculating some of the bounds given by experiment. Additionally, the cutflow for a selection of signal regions was reproduced by an independent implementation within uncertainties.

With our setup we will consider the following production processes $pp \to \chi^0\bar{\chi}^0$, $pp \to \chi^0\chi^+$, $\chi^-\bar{\chi}^0$, $pp \to \chi^0\rho^-, \rho^+\bar{\chi}^0$, $pp \to \tilde{\ell}^+_R\tilde{\ell}^-_R$. The corresponding production cross sections of our benchmark points are given in Tab. 4. Processes with left-handed sleptons are neglected, assuming that the masses are above the detection limit as discussed before. The masses of the relevant particles are given in Tab. 5.

In the next sections we will show how the setup described here is used to recast the experimental bounds on the chargino and neutralino sector of the MRSSM. We will also highlight differences to the usual MSSM interpretations.

[3] `Herwig++`-2.7 is used with default settings, underlying event tune (UE-EE-5-MRST [79]) and PDF set (LO^* from [80]).

[4] With `CheckMATE` we make use of `Delphes` 3 [82], `FastJet` [83], the anti-k_t clustering [84, 85], and the CL_s description [86].

	χ_1^0	χ_2^0	χ_3^0	χ_4^0	$\chi_1^\pm$	$\chi_2^\pm$	$\rho_1^\pm$	$\rho_2^\pm$	$\tilde{\tau}_R$	$\tilde{\mu}_R$	$\tilde{e}_R$	$\tilde{\ell}_L$	m_{H_1}
BMP4	49.8	132	617	691	131	625	614	713	128	802	802	808	100
BMP5	43.9	401	519	589	409	524	519	610	1000	1001	1001	1005	94
BMP6	29.7	427	562	579	422	562	433	587	106	353	353	508	95

Table 5. Masses of the non-SM particles in the BMPs relevant for the LHC studies discussed here. All values given in GeV.

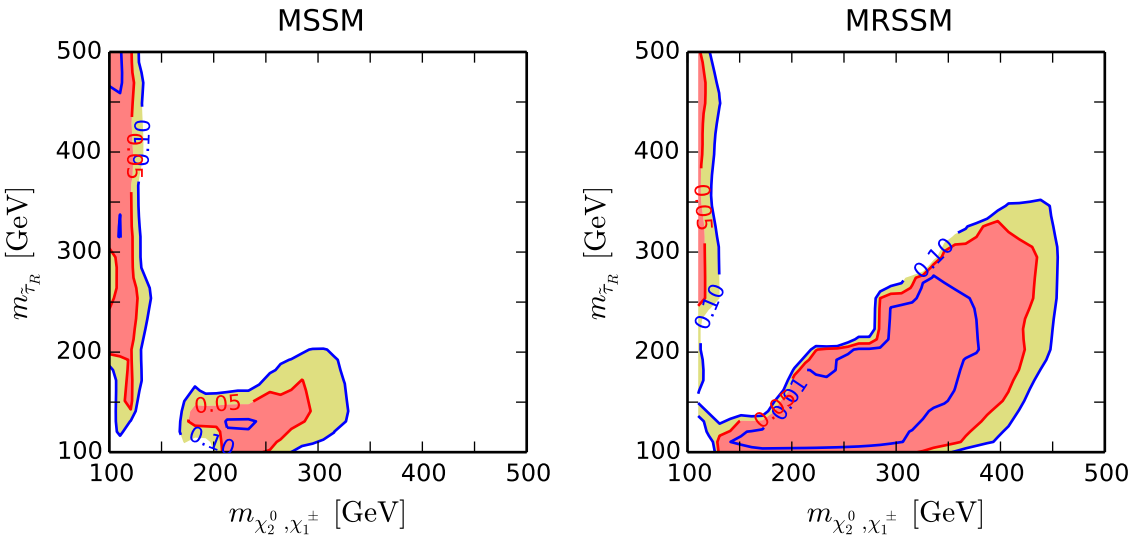

Figure 3. Exclusion plots in the chargino-neutralino and stau mass plane for the first scenario of Tab. 3 in the MSSM (left) and in the MRSSM (right).

3.4 Light staus and light charginos

In the following we focus on specific cases, which are of interest for the light-singlet scenario and which are promising in view of dark matter. We begin with the case corresponding to the first row of Table 3, i.e. we consider a very light LSP (a bino-like in the MSSM, and a bino-singlino in the MRSSM), and a relatively light chargino (a wino in the MSSM, and a down-(R-)higgsino in the MRSSM). We also take relatively light staus, which are motivated by dark matter considerations.

Fig. 3 shows the resulting exclusion plots taking into account the experimental analyses as discussed in the last section. The results show striking differences between the MSSM and the MRSSM cases. In the MSSM the produced charginos are wino-like and all possible decay channels (Higgs, W/Z, staus) can contribute with comparable size to their total width. Therefore, as none of the signal regions of the analyses performed by the LHC experiments have been designed to accept all events/scenarios, the derived limits are rather weak. Especially for $m_{\chi_2^0} > m_{\chi_1^0} + m_h$ the decay to Higgs channel is dominant. The experimental analyses used here rely on final states with charged leptons and are not

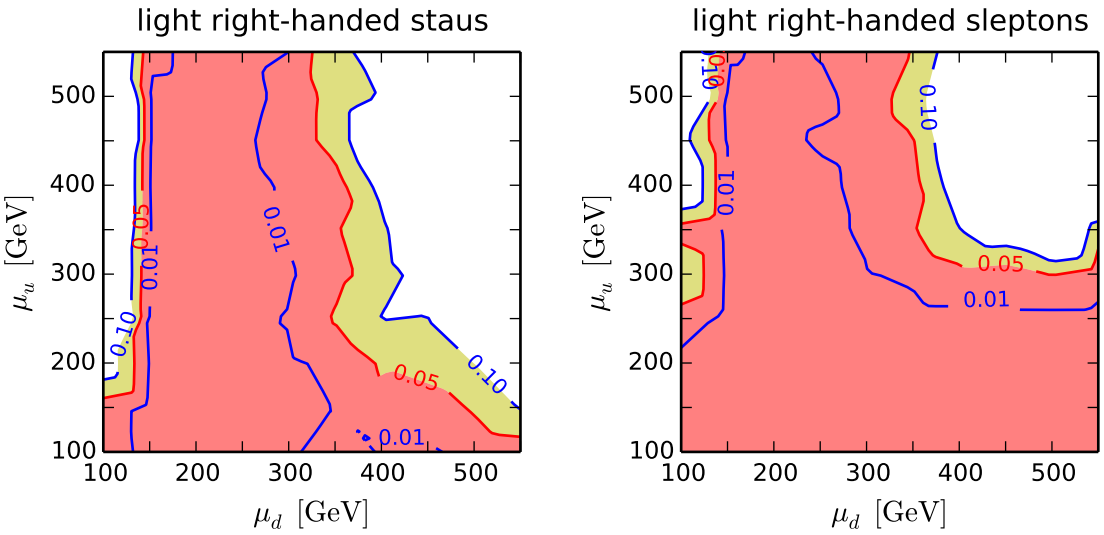

Figure 4. Exclusion limits in the MRSSM for light staus as a function of the two higgsino mass parameters $\mu_{d,u}$. The red (yellow) region marks the 95% (90%) excluded parameter region, computed as described in the text. The left plot has light right-handed stau mass of 100 GeV, in the right plot all right-handed slepton masses are set to 100 GeV. All other parameters are fixed to the values of BMP5. Most importantly, the Dirac wino mass is set to $M_W^D = 500$ GeV.

sensitive to Higgs bosons in the final state, yielding a low exclusion power.[5] Only two small regions are excluded: the region with a chargino mass below 100–150 GeV (depending on the stau mass), and the region around the chargino mass of 150–300 GeV and stau mass below 150 GeV. In contrast, for the MRSSM the produced charginos are down-higgsino-like and the decay to stau, if available, is preferred. This makes the searches designed for events with large multiplicity of taus very efficient. Hence, a large triangular region with chargino mass between the decay threshold ($m_{\tilde{\tau}_R} + m_{\rm LSP}$) and around 450 GeV is excluded. Interestingly, however, to the left of the triangle the chargino becomes too light, decays to on-shell staus are impossible, and decays via off-shell stau are suppressed. In that region the acceptance is lowered and with present Run-I data no exclusion is possible.

3.5 General investigation of light charginos

Now we discuss the limits on chargino and neutralino masses in more generality. Fixing the bino-singlino to be very light, ~ 50 GeV, there are three relevant mass parameters: the Dirac wino-triplino mass M_W^D and the two higgsino masses $\mu_{d,u}$. Further, the exclusion limits depend on the slepton masses.

Figure 4 shows the exclusion regions in the plane of the two higgsino masses μ_d–μ_u, for the case that also right-handed staus are light. In the left plot all other sleptons are heavy; in the right plot the right-handed sleptons of the other generations are also light. In both

[5] Dedicated analyses taking Higgs bosons in the final state into account exist but are not implemented in the used version of `CheckMATE` [74, 93].

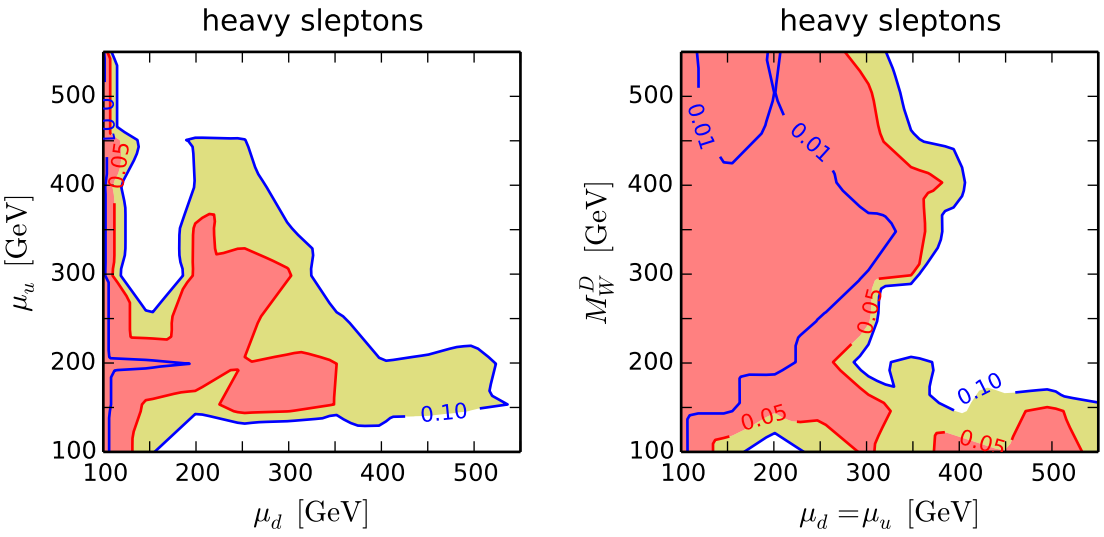

Figure 5. Exclusion limits in the MRSSM for heavy sleptons as a function of the two higgsino masses (left) and of the higgsino and wino-triplino masses (right). The red (yellow) region marks the 95% (90%) excluded parameter region. All parameters which are not varied in the plots are fixed to the values of BMP5.

plots there is an interesting non-excluded region with very small μ_d, below around 150 GeV. This is consistent with the discussion of the previous subsection and with the corresponding region in Fig. 3. The region for μ_d between around 150 and 400 GeV corresponds to the triangular region in Fig. 3, in which the decay of the higgsino into stau is dominant, and is excluded. In the case of light right-handed sleptons of all generations, the region for the other higgsino mass μ_u below around 300 GeV is also excluded. This originates from the mixing with the bino, leading to non-negligible and democratically distributed decay to all right-handed sleptons in addition to the decay to Z and Higgs boson. Therefore selectrons and smuons will be produced in large enough abundance to be picked up by the experiments. As discussed before, this is in contrast to the down-higgsino, where the mixing to the bino is suppressed via large $\tan\beta$ and the large Yukawa coupling of tau leads to dominating decay into staus. In the case of heavy sleptons of the first two generations, the exclusion power on μ_u is very weak as the decay to Z and Higgs boson have comparable branching ratios. Thus the case of light right-handed staus leads to two distinct viable parameter regions, one with very small μ_d and one with larger μ_d. These two regions are represented by the two benchmark points BMP4 and BMP6.

Now we consider the case in which all sleptons, including the staus, are heavy. Figure 5 shows the exclusion regions for this case, once in the $\mu_d - \mu_u$ plane (with $M_W^D = 500$ GeV), and once in the $\mu_d{=}\mu_u - M_W^D$ plane. Both plots show that once both higgsinos are heavier than around 300 GeV there are parameter regions that are safe from exclusion. This generic, viable parameter region for heavy sleptons is represented by benchmark point BMP5.

The left plot of Fig. 5 analyzes the case that one of the higgsinos is lighter. It shows two additional strips of parameter space at higgsino masses around 150 GeV, which are not

excluded by the considered LHC searches. The physics reason for the existence of these regions are the higgsino decay patterns. In the non-excluded strips the dominant decay of the light higgsino is a two-body decay into the LSP and W/Z or SM-like Higgs boson. Due to the small higgsino mass, the LSP is too soft to allow a discrimination of the events from the background of standard on-shell W/Z/Higgs production and decay. For even lower higgsino masses, the dominant decay modes are 3-body decays via the SM bosons. In this case the SM background for the lepton searches is smaller and the exclusion power higher. We exemplify the region of low μ_d by the benchmark point BMP4. For the region of low μ_u we also need to consider constraints from dark matter searches, which will be described in the next section.

In the right of Fig. 5 masses of the wino-triplino M_W^D below 200 GeV for higgsino masses above 300 GeV can not be excluded by the analyses used here. As was discussed before, the wino-triplino decays predominantly into Higgs bosons and LSP and the Higgs boson again mainly into bottom quarks. As described before, this gives a low exclusion power since the experimental analyses so far are not sensitive to the Higgs bosons in the final state.

In summary, our investigations show that there are three qualitatively different viable parameter regions compatible with very light bino-singlino state, represented by the three benchmark points BMP4,5,6. Two regions are characterized by light right-handed stau and either light or heavy down-higgsino (where light/heavy means masses around 100 GeV/larger than around 400 GeV, respectively). The third region is characterized by generally heavy sleptons and higgsino masses above around 300 GeV. In all cases, the wino-triplino mass is not very critical; the benchmark points have M_W^D between 400–600 GeV, but smaller values are allowed as well, and do not give rise to a different phenomenology.

4 Dark matter constraints

As was pointed out in Sec. 2 the scenario with a light singlet Higgs state considered in this work leads to an upper bound on the bino-singlino mass parameter $M_B^D < 55$ GeV. The neutralino, which is mainly given by this component, will become the LSP. Therefore, it is the dark matter candidate of our model and we will study here how viable this scenario is when confronted with constraints from dark matter searches. Dirac neutralinos as a candidate for dark matter were already studied in Ref. [34, 36]. Especially in Ref. [36] it was clarified that the bino-singlino state is viable candidate as it is possible to achieve the correct relic abundance by annihilation to leptons through sleptons, especially a light right-handed stau. Additionally, the spin-independent direct detection channels were investigated and the squark and Z boson exchange as main contributions were identified. Interference between those two channels was neglected, but we will see in the following that it plays an important role to evade the direct detection limits.

The technical setup for the numerical computations described below is as follows. We use `MicrOMEGAs`-4.1.8 [94] to calculate the relic density and direct detection rate for the MRSSM. The model input is given by the `CalcHEP` output of `SARAH` and for each parameter point the mass spectrum and couplings calculated with `SPheno` at full one-loop level is passed to the program. For the comparison to the experimental data and statistical inter-

	BMP4	BMP5	BMP6
m_{χ^1}	49.8 GeV	43.9 GeV	29.7 GeV
$m_{\tilde{\tau}_R}$	128.5 GeV	1 TeV	105.6 GeV
Ωh^2	0.119	0.092	0.127
direct detection p-value	0.9	0.5	0.2

Table 6. Values of dark matter observables for the benchmark points.

pretation of the direct detection part we use `LUXCalc` [95], which uses results from the LUX experiment [96], and input on the cross section for each parameter point from `MicrOMEGAs`.

4.1 Relic density

We first consider the question which parameter space of the light-singlet scenario is compatible with the measured dark matter relic density. As in the MSSM, the crucial requirement is to achieve sufficiently effective LSP pair annihilation processes. In the parameter regions found in the previous sections, it turns out that two cases are promising. Either, if the condition $m_{\chi_1} \approx M_Z/2$ is valid and S-channel resonant LSP pair annihilation into Z bosons is possible, or if right-handed staus are light and enable annihilation via t-channel stau exchange into tau leptons, see the corresponding Feynman diagrams in Fig. 6, when $f, \tilde{f}$ replaced by $\tau, \tilde{\tau}$ for non-Z-exchange diagrams.

Fig. 7 (left) shows the resulting allowed contour in the M_B^D–$m_{\tilde{\tau}_R}$ parameter space. In the plot, all non-varied parameters are fixed to the values of BMP6, but this choice is not crucial. The important feature is that, as in the MSSM, to meet the measured value of the relic density the stau mass has to lie in a small interval once the other parameters are given. The contour has a sharp resonance-like peak around $M_B^D \approx M_Z/2$ which results from the S-channel annihilation process. The two different possibilities mentioned above correspond to being at the resonance or away from it.

In the resonance peak the required stau mass has to be rather high. This is the situation realized in our benchmark point BMP5. For this scenario to be viable it has to be ensured that the Z boson does not decay to the LSP with a detectable effect to the invisible width of the Z boson. Since the same interaction is also important for, and thus constrained by, the direct detection cross section, we will discuss it in the subsequent subsection.

For values of M_B^D away from the resonance, Fig. 7 (left) shows that the required stau mass is small and below 150 GeV. The benchmark points BMP4 and BMP6 represent this case. For such light staus the LEP bound on the stau mass of ≈ 82 GeV [97] needs to be taken into account. In general, the LEP bound implies that there is a lower limit on M_B^D for which the dark matter density can be explained.

Table 6 provides the precise values for the LSP and right-handed stau masses, as well as the relic density, for the benchmark points. Again the different characteristics of BMP5 and BMP4/BMP6 are visible. The benchmark point BMP4 has been tuned to give exactly the experimental value of $\Omega h^2 = 0.1199 \pm 0.0027$ [98]. For BMP5 (BMP6) the bino-singlino

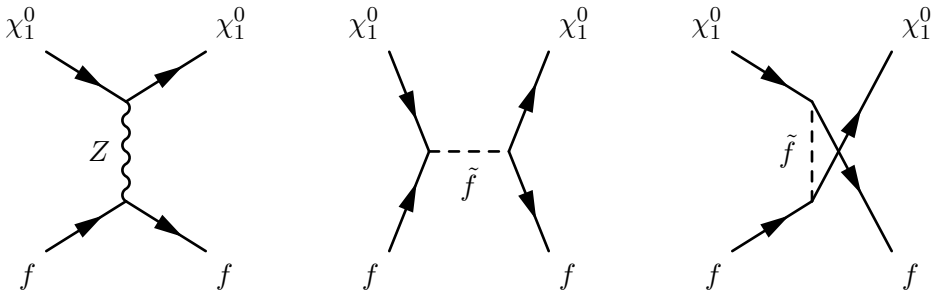

Figure 6. Feynman diagrams for the most relevant LSP annihilation (with $f, \tilde{f}$ replaced by $\tau, \tilde{\tau}$) and direct detection processes ($f, \tilde{f}$ replaced by $u, \tilde{u}$ and $d, \tilde{d}$).

(stau) mass can easily be tuned by a small percentage to achieve full agreement with the measured Ωh^2.

4.2 Direct detection

The spin-independent dark matter–nucleon scattering cross section can be given in terms of two scattering amplitudes f_p, f_n. These are conventionally normalized such that the total spin-independent cross section at zero momentum transfer is

$$\sigma_{DM-N} = \frac{4\mu_{Z_A}^2}{\pi} \left(Z f_p + (A - Z) f_n\right)^2 . \tag{4.1}$$

Here $\mu_{Z_A}^2$ is the dark matter–nucleon reduced mass, and A and Z are atomic mass and number, respectively.

As noted in Ref. [36], the spin-independent cross-section for Dirac neutralinos is dominated by the vector part of the Z boson-exchange and squark-exchange contributions. The relevant Feynman diagrams are shown in Fig. 6, when $f, \tilde{f}$ replaced by $u, \tilde{u}$ and $d, \tilde{d}$. Each contribution can lead to large scattering rates and thus to strong bounds on the parameter space. For this reason we provide explicit expressions for the relevant amplitudes. For the Z-mediated diagram we obtain

$$f_p^{\text{Z boson}} = \frac{-g_2^2}{8 m_Z^2 c_W^2} \left(\frac{1}{2} - 2 s_W^2\right) \left(\frac{Z_{1,3-4} + Z_{2,3-4}}{2}\right) , \tag{4.2}$$

$$f_n^{\text{Z boson}} = \frac{g_2^2}{16 m_Z^2 c_W^2} \left(\frac{Z_{1,3-4} + Z_{2,3-4}}{2}\right) , \tag{4.3}$$

where $Z_{i,3-4} = (N_{13}^i)^2 - (N_{14}^i)^2$ is the difference of the mixing matrix elements squared for the mixing of the bino with the down- and up-R-higgsino (singlino with the down- and up-higgsino) when $i = 1$ ($i = 2$), see Eqs. (A.2) and (A.3). Here we also use the shorthand notation $s_W = \sin\theta_W$, $c_W = \cos\theta_W$.

The coupling factors $Z_{i,3-4}$ arise because the Z boson only couples to the (R-)higgsino content of the LSP. Qualitatively, in order to suppress these amplitudes and to ensure agreement with current direct detection bounds, the (R-)higgsino mix-in to the LSP has to be suppressed. This leads particularly to constraints on the higgsino mass parameters μ_u

and μ_d. As a simple illustration, we assume $\tan\beta \gg 1$, $\lambda_u = 0$, and $\mu_u \gg M_B^D, g_1 v$ and further that the direct mixing between up-higgsino and bino will be dominant. In this case, the mixing matrix elements appearing in Eqs. (4.2) and (4.3) take the form

$$Z_{1,3-4} + Z_{2,3-4} = -\left(\frac{g_1 v}{2\mu_u}\right)^2 , \tag{4.4}$$

clearly exhibiting the suppression by large μ_u. Similarly, we have evaluated the squark-mediated diagrams of Fig. 6 for general masses of the four first-generation squarks, $\tilde{u}_L$, $\tilde{u}_R$, $\tilde{d}_L$, $\tilde{d}_R$. For the qualitative discussion it is sufficient to provide the results in the limit of heavy squarks of equal mass $m_{\tilde{q}} = m_{\tilde{d}} \approx m_{\tilde{u}} \gg m_{\chi_1}$. In this limit we obtain

$$f_p^{\text{heavy squark}} = \frac{g_1^2}{4m_{\tilde{q}}^2}\left[\left(\frac{4}{9} - \frac{1}{36}\right) + \frac{1}{2}\left(\frac{1}{9} - \frac{1}{36}\right)\right], \tag{4.5}$$

$$f_n^{\text{heavy squark}} = \frac{g_1^2}{4m_{\tilde{q}}^2}\left[\frac{1}{2}\left(\frac{4}{9} - \frac{1}{36}\right) + \left(\frac{1}{9} - \frac{1}{36}\right)\right]. \tag{4.6}$$

The minus signs result from the different Dirac structure of the S and U channels that contribute to the process. Therefore, in order to suppress these amplitudes and ensure agreement with current bounds, the squarks need to be sufficiently heavy.[6]

For our quantitative evaluation we include the full experimental information from LUX by using `LUXCalc` and the complete theoretical prediction of the proton and neutron scattering amplitudes. A likelihood is then constructed from Poisson distribution

$$\mathcal{L}\left(m_\chi, \{f_N\}|N\right) = \frac{(\mu + b)^N e^{-(\mu+b)}}{N!}, \tag{4.7}$$

where N and b are the observed and expected numbers of events by the LUX experiment, respectively, and μ is the expected number of signal events for a given WIMP mass and its effective couplings. Furthermore, we assume that DM consists in equal proportions from χ and $\bar{\chi}$ and use default settings for the halo profile in `MicrOMEGAs`.

On the right of Fig. 7, the 95 % and 90 % exclusion bounds (violet (dark) and yellow (light dark) regions) derived using the log likelihood for the direct detection by LUX given in Eq. (4.7) are shown depending on μ_u and the first/second generation squark masses. Here, it can be seen that the derived limits are quite sensitive to the combination of both parameters. This dependence stems from an interference of the amplitudes and can be understood by a simplified analysis of the expressions, as given before.

In the approximation leading to Eq. (4.4), we can add the Z- and squark-exchange contributions to a simple form

$$f_n^{\text{Z boson+heavy squark}} = \frac{g_1^2}{96}\left(\frac{7}{m_{\tilde{q}}^2} - \frac{3}{\mu_u^2}\right), \quad f_p^{\text{Z boson+heavy squark}} = \frac{g_1^2}{96}\left(\frac{11}{m_{\tilde{q}}^2}\right), \tag{4.8}$$

[6] Our expressions for the direct detection amplitudes differ by a factor 1/16 in Eqs. (4.2,4.3) and by the relative sign between the left-handed and right-handed squark contributions in Eqs. (4.5,4.6) from the corresponding ones of Ref. [36].

where $s_W^2 = 1/4$ has been taken in the proton case. Plugging these results into the expression for the dark matter–nucleus cross section, Eq. (4.1), we find a complete destructive interference, i.e. $\sigma_{DM-N} = 0$, when

$$m_{\tilde{q}} = \sqrt{\frac{7 + 11\frac{A}{Z-A}}{3}}\mu_u \overset{\text{Xe}}{\approx} 2.2\mu_u \ , \tag{4.9}$$

where the numerical value for xenon is calculated with $A = 54$ and $Z = 131.3$.

The line of destructive interference corresponding to Eq. (4.9), shown as a full line in Fig. 7 (right), explains the funnel-shaped allowed region. Above the line, the squark-mediated amplitudes become small, to the right of the line, the Z-mediated amplitudes become small. It should be noted that the result for the exclusion bounds is calculated using the complete information of `micrOMEGAs` and `LUXCalc`, while Eq. (4.9) is only approximated. As the squark masses of the first two generations are limited by LHC searches, the direct detection non-discovery provides a lower limit on μ_u. This also excludes the region of low μ_u allowed by LHC searches in the left of Fig. 5.

As discussed before, the amplitude for the Z-mediated exchange is closely related to one responsible for the Z boson decay to a pair of LSP. Both depend strongly on the $Z_{i,3-4}$ containing the neutralino mixing matrix elements. The direct detection limit of Fig. 7 limits the $Z_{i,3-4}$ strongly enough so that $\Gamma(Z \to \chi_1^0\bar{\chi}_1^0) \ll 3$ MeV is ensured over all the parameter space.

Xenon is not the only element used for direct detection experiments, therefore the change of the values of A and Z has to be taken into account, when using Eq. (4.9) for other cases. The variation of the ratio $A/(Z - A)$ (0.7 for xenon, 0.8 for argon and germanium) is small enough that the regions of strong destructive interference for different experiments will not overlap in the MRSSM parameter space. Here, we only take the LUX result into account as it is the most sensitive one available.

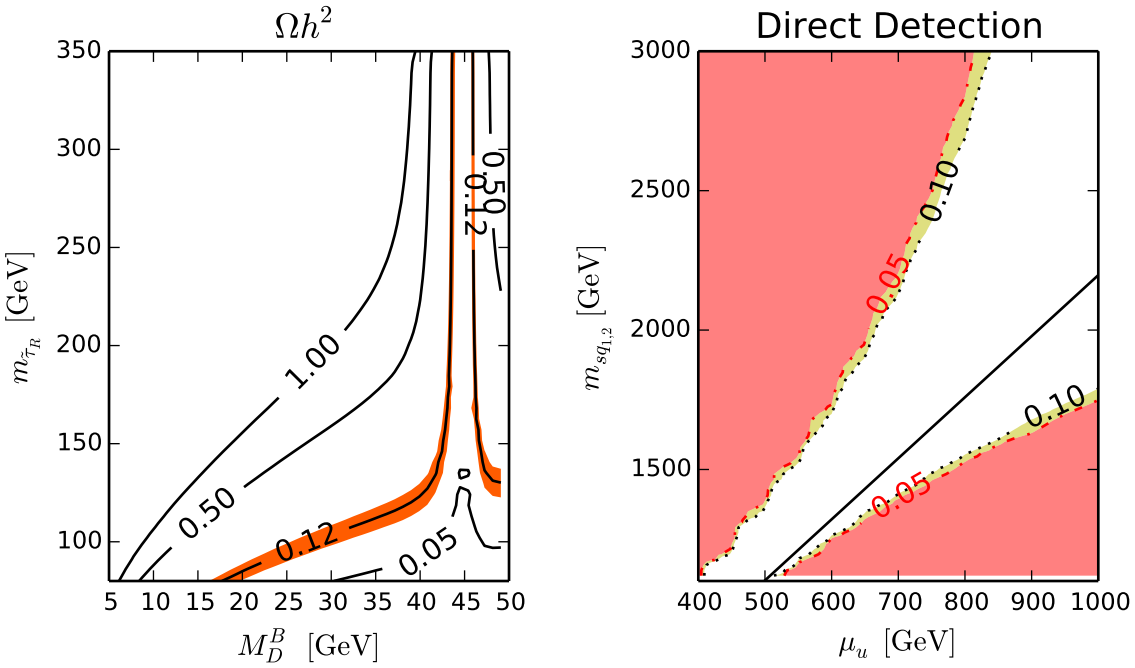

Figure 7. Dark matter relic density as a function of the bino mass parameter and right-handed slepton masses (left). Exclusion limits in the MRSSM depending on μ_u and equal first and second generation squark masses (right) from direct detection. The red with dashed dotted border (yellow with dotted border) region marks the 95% (90%) excluded parameter region calculated with `micrOMEGAs` and `LUXcalc`. The full line shows the approximation relation for the full destructive interference in Eq. (4.9). The non-varied parameters in each plot are fixed to the values of BMP6.

5 Summary and conclusions

The minimal R-symmetric model MRSSM is a promising alternative to the MSSM, which predicts Dirac gauginos and higgsinos as well as scalars in the adjoint representation of SU(3)×SU(2)×U(1). Here we have investigated the possibility that the scalar singlet mass is small and gives rise to a singlet-like mass eigenstate with mass below 125 GeV. The potential advantages of this scenario are an increased tree-level SM-like Higgs boson mass, many light weakly interacting particles which could be discovered at the next LHC run, and the possibility to explain dark matter.

Many of the model parameters are strongly constrained in order to make this scenario viable. Here we briefly summarize the main constraints. Fig. 8 summarize the four most important non-LHC constraints on the relevant parameters. There, the SM-like Higgs boson mass is given by the green-yellow colour bands, while the red area shows the regions excluded by direct detection searches. Black full (blue dashed) lines give the W boson mass (Ωh^2) contours. All plots are based on BMP6, except for Fig. 8(d), where BMP4 was used.

In order to realize a light singlet-like Higgs boson in the first place, not only the parameter m_S but also M_B^D and λ_u must be very small. The SM-like Higgs boson mass is increased at tree-level compared to the case with heavy singlet or to the MSSM, but loop

contributions governed by Λ_u are still important. Accordingly, the plots of Fig. 8 show that the Higgs mass measurement essentially fixes Λ_u and constrains M_B^D and μ_u. We have found that the other constraints in Higgs physics, arising from measurements of Higgs properties and of non-discovery of further Higgs states, can be easily fulfilled. As discussed in Ref. [46], the W-boson mass can be explained simultaneously with the SM-like Higgs boson mass. Fig. 8 confirms that this is still the case in the light singlet scenario.

The dark matter relic density can be explained in the MRSSM light singlet scenario because the Dirac bino-singlino neutralino is necessarily the stable LSP. Agreement with the observed relic density requires particular combinations of the bino-singlino mass M_B^D and the right-handed stau mass. If the latter is heavy, as in our benchmark point BMP5, the LSP mass must be close to half of the Z boson mass. If the LSP mass is away from the Z boson resonance, the right-handed stau must be light, as in our BMP4 and BMP6. This resonance behaviour is clearly displayed in Fig. 8(a). Parameters like μ_u, μ_d influence the relic density due to their impact on the LSP mass via mixing, Fig. 8(d).

Further bounds on the model parameters arise from the negative searches for dark matter and from the negative LHC searches for SUSY particles. The direct dark matter searches correlate μ_u with $m^2_{\tilde{q}_R;1,2}$, Fig. 8(b). Because of the non-discovery of squarks at LHC so far, this give rise to a lower bound on μ_u, which is not affected by other parameters of the weak sector like Λ_u, Fig. 8(c). Together with the Higgs mass value, however, these searches constrain both μ_u and $m^2_{\tilde{q}_R;1,2}$ to a rather narrow range, see Fig. 8(b).

Our recast of LHC analyses has revealed three distinct viable parameter regions of interest, represented by the three benchmark parameter points BMP4, BMP5, BMP6. The most obvious region is characterized by heavy M_W^D, μ_d and sleptons (BMP5). A second is characterized by very light right-handed stau mass around 100 GeV (BMP6); in the third region the right-handed stau and μ_d are very light (BMP4). Fig. 8(d), which gives the parameter variation for BMP4, shows that this region is also allowed by the other constraints. As explained in Sec. 3, these two regions are allowed because the existing LHC searches become ineffective. The LHC searches alone would allow further parameter regions with very small μ_u, which however are excluded by dark matter constraints.

To summarize: the experimental data from collider and dark matter experiments impose stringent constraints on the parameter of the light scalar scenario of the MRSSM. Nevertheless we have identified regions in the parameter space and proposed representative benchmark points fulfilling all the constraints. All viable parameter regions are characterized by several light weakly interacting SUSY particles and will be tested both by future dark matter and LHC SUSY searches.

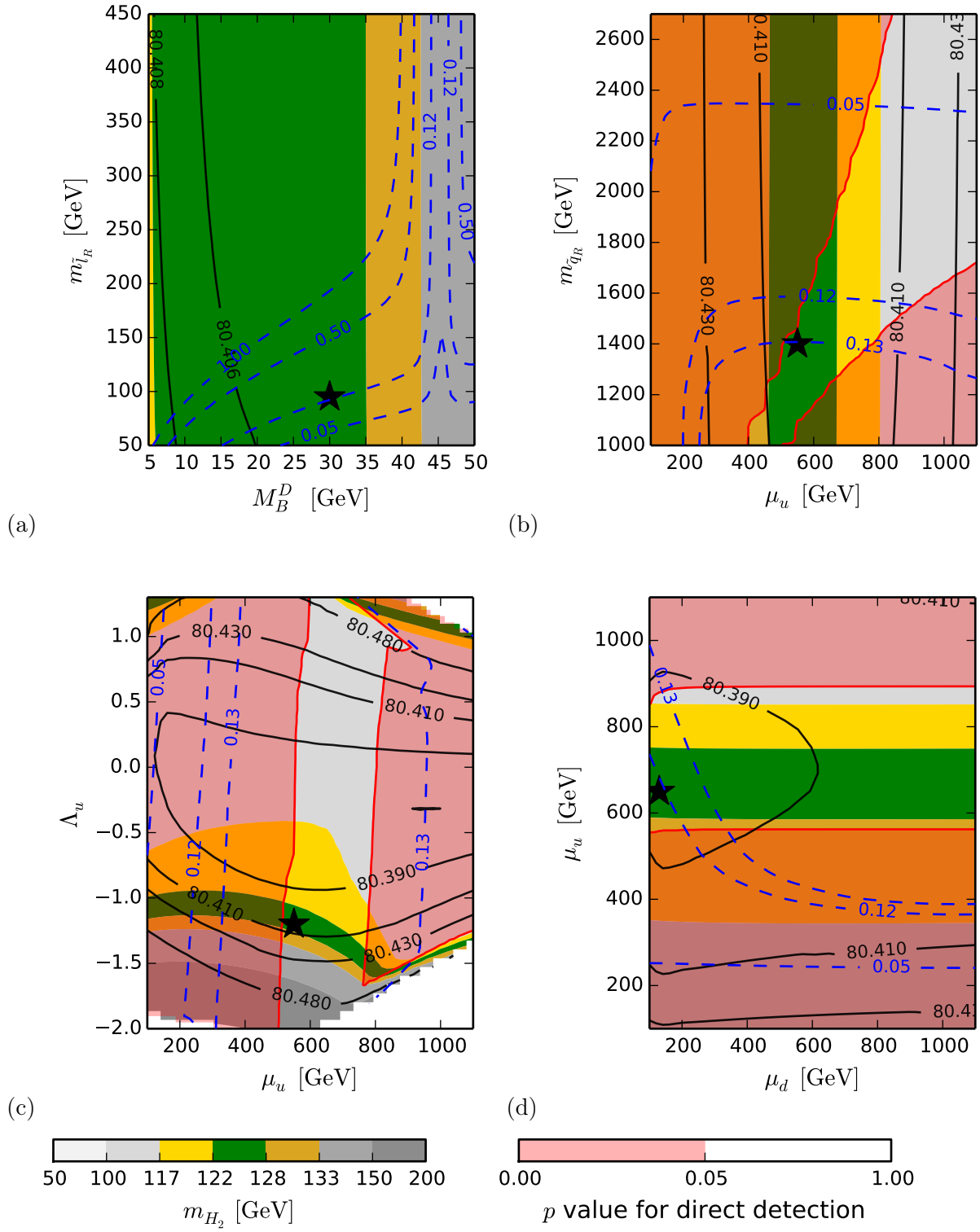

Figure 8. Shown are parameter regions and their agreement with experiment. Red overlaid areas are excluded with 95% CL by dark matter direct detection. Black full (blue dashed) lines show m_W (Ωh^2). The mass of the SM-like Higgs boson m_{H_2} is given by the colour scale shown. All non-varied parameters are set to the values of BMP6, except for the bottom right plot, where BMP4 is used. BMPs are marked by stars. The white areas in (d) stem from tachyonic states appearing in the mass spectrum, at the borders to these areas the interpolation breaks down.

Acknowledgments

Work supported in part by the German DFG Research Training Group 1504 and the DFG grant STO 876/4-1, the Polish National Science Centre grants under OPUS-2012/05/B/ST2/03306 and the European Commission through the contract PITN-GA-2012-316704 (HIGGSTOOLS).

WK would like to thank Aleksandra Drozd for useful discussions concerning dark matter. PD would like to thank Daniel Schmeier for technical support with `CheckMATE`. We thank Christopher Savage for help on `LUXCalc` usage in the case of Dirac dark matter candidate.

A MRSSM mass matrices at tree level

For completeness we recall here the tree-level mass matrices for the Higgs bosons and the charginos and neutralinos of the MRSSM, which are relevant for the discussion of the present paper.

a) Pseudo-scalar Higgs bosons:
Since in the pseudo-scalar sector of $(\sigma_d, \sigma_u, \sigma_S, \sigma_T)$ there is no mixing between the MSSM-like states (σ_d, σ_u) and the singlet-triplet states (σ_S, σ_T), the mass-squared matrix breaks into two 2x2 submatrices as follows

$$\mathcal{M}^{\sigma}_{u,d} = \begin{pmatrix} B_\mu \frac{v_u}{v_d} & B_\mu \\ B_\mu & B_\mu \frac{v_d}{v_u} \end{pmatrix}, \qquad \mathcal{M}^{\sigma}_{S,T} = \begin{pmatrix} m_S^2 + \frac{\lambda_d^2 v_d^2 + \lambda_u^2 v_u^2}{2} & \frac{\lambda_d \Lambda_d v_d^2 - \lambda_u \Lambda_u v_u^2}{2\sqrt{2}} \\ \frac{\lambda_d \Lambda_d v_d^2 - \lambda_u \Lambda_u v_u^2}{2\sqrt{2}} & m_T^2 + \frac{\Lambda_d^2 v_d^2 + \Lambda_u^2 v_u^2}{4} \end{pmatrix}. \tag{A.1}$$

b) Neutralinos:
In the weak basis of eight neutral electroweak two-component fermions: $\xi_i = (\tilde{B}, \tilde{W}^0, \tilde{R}_d^0, \tilde{R}_u^0)$, $\zeta_i = (\tilde{S}, \tilde{T}^0, \tilde{H}_d^0, \tilde{H}_u^0)$ with R-charges $+1$, -1 respectively, the neutralino mass matrix takes the form of

$$m_\chi = \begin{pmatrix} M_B^D & 0 & -\frac{1}{2} g_1 v_d & \frac{1}{2} g_1 v_u \\ 0 & M_W^D & \frac{1}{2} g_2 v_d & -\frac{1}{2} g_2 v_u \\ -\frac{1}{\sqrt{2}} \lambda_d v_d & -\frac{1}{2} \Lambda_d v_d & -\mu_d^{\text{eff},+} & 0 \\ \frac{1}{\sqrt{2}} \lambda_u v_u & -\frac{1}{2} \Lambda_u v_u & 0 & \mu_u^{\text{eff},-} \end{pmatrix}. \tag{A.2}$$

The transformation to a diagonal mass matrix and mass eigenstates κ_i and ψ_i is performed by two unitary mixing matrices N^1 and N^2 as

$$N^{1,*} m_\chi N^{2,\dagger} = m_\chi^{diag}\,, \qquad \xi_i = \sum_{j=1}^{4} N_{ji}^{1,*} \kappa_j\,, \qquad \zeta_i = \sum_{j=1}^{4} N_{ij}^{2,*} \psi_j\,,$$

and physical four-component Dirac neutralinos are constructed as

$$\chi_i^0 = \begin{pmatrix} \kappa_i \\ \psi_i^* \end{pmatrix} \qquad i = 1, 2, 3, 4. \tag{A.3}$$

c) Charginos:
The mass matrix of charginos in the weak basis of eight charged two-component fermions

breaks into two 2x2 submatrices. The first, in the basis $(\tilde{T}^-, \tilde{H}_d^-), (\tilde{W}^+, \tilde{R}_d^+)$ of spinors with R-charge equal to electric charge, takes the form of

$$m_{\chi^+} = \begin{pmatrix} g_2 v_T + M_W^D & \frac{1}{\sqrt{2}}\Lambda_d v_d \\ \frac{1}{\sqrt{2}} g_2 v_d & +\mu_d^{\text{eff},-} \end{pmatrix} \tag{A.4}$$

The diagonalization and transformation to mass eigenstates $\lambda_i^\pm$ is performed by two unitary matrices U^1 and V^1 as

$$U^{1,*} m_{\chi^+} V^{1,\dagger} = m_{\chi^+}^{diag}\,, \qquad \tilde{T}^- = \sum_{j=1}^{2} U_{j1}^{1,*} \lambda_j^-\,, \qquad \tilde{H}_d^- = \sum_{j=1}^{2} U_{j2}^{1,*} \lambda_j^-\,, \tag{A.5}$$

$$\tilde{W}^+ = \sum_{j=1}^{2} V_{1j}^{1,*} \lambda_j^+\,, \qquad R_d^+ = \sum_{j=1}^{2} V_{2j}^{1,*} \lambda_j^+ \tag{A.6}$$

and the corresponding physical four-component charginos are built as

$$\chi_i^+ = \begin{pmatrix} \lambda_i^+ \\ \lambda_i^{-*} \end{pmatrix} \qquad i = 1, 2. \tag{A.7}$$

The second submatrix, in the basis $(\tilde{W}^-, R_u^-)$, $(\tilde{T}^+, \tilde{H}_u^+)$ of spinors with R-charge equal to minus electric charge, reads

$$m_{\rho^-} = \begin{pmatrix} -g_2 v_T + M_W^D & \frac{1}{\sqrt{2}} g_2 v_u \\ -\frac{1}{\sqrt{2}}\Lambda_u v_u & -\mu_u^{\text{eff},+} \end{pmatrix} \tag{A.8}$$

The diagonalization and transformation to mass eigenstates $\eta_i^\pm$ is performed by U^2 and V^2 as

$$U^{2,*} m_{\rho^-} V^{2,\dagger} = m_{\rho^-}^{diag}\,, \qquad \tilde{W}^- = \sum_{j=1}^{2} U_{j1}^{2,*} \eta_j^-\,, \qquad R_u^- = \sum_{j=1}^{2} U_{j2}^{2,*} \eta_j^- \tag{A.9}$$

$$\tilde{T}^+ = \sum_{j=1}^{2} V_{1j}^{2,*} \eta_j^+\,, \qquad \tilde{H}_u^+ = \sum_{j=1}^{2} V_{2j}^{2,*} \eta_j^+ \tag{A.10}$$

and the other two physical four-component charginos are built as

$$\rho_i^- = \begin{pmatrix} \eta_i^- \\ \eta_i^{+*} \end{pmatrix} \qquad i = 1, 2. \tag{A.11}$$

References

[1] G. Aad *et al.* [ATLAS Collaboration], Phys. Lett. B **716** (2012) 1 doi:10.1016/j.physletb.2012.08.020 [arXiv:1207.7214 [hep-ex]].

[2] S. Chatrchyan *et al.* [CMS Collaboration], Phys. Lett. B **716** (2012) 30 doi:10.1016/j.physletb.2012.08.021 [arXiv:1207.7235 [hep-ex]].

[3] The ATLAS and CMS Collaborations, ATLAS-CONF-2015-044.

[4] S. Heinemeyer, O. Stal and G. Weiglein, Phys. Lett. B **710** (2012) 201 doi:10.1016/j.physletb.2012.02.084 [arXiv:1112.3026 [hep-ph]].

[5] R. Benbrik, M. Gomez Bock, S. Heinemeyer, O. Stal, G. Weiglein and L. Zeune, Eur. Phys. J. C **72** (2012) 2171 doi:10.1140/epjc/s10052-012-2171-2 [arXiv:1207.1096 [hep-ph]].

[6] P. Bechtle, S. Heinemeyer, O. Stal, T. Stefaniak, G. Weiglein and L. Zeune, Eur. Phys. J. C **73** (2013) 4, 2354 doi:10.1140/epjc/s10052-013-2354-5 [arXiv:1211.1955 [hep-ph]].

[7] U. Ellwanger, C. Hugonie and A. M. Teixeira, Phys. Rept. **496** (2010) 1 doi:10.1016/j.physrep.2010.07.001 [arXiv:0910.1785 [hep-ph]].

[8] M. Maniatis, Int. J. Mod. Phys. A **25** (2010) 3505 doi:10.1142/S0217751X10049827 [arXiv:0906.0777 [hep-ph]].

[9] Z. Kang, J. Li and T. Li, JHEP **1211** (2012) 024 doi:10.1007/JHEP11(2012)024 [arXiv:1201.5305 [hep-ph]].

[10] D. A. Vasquez, G. Belanger, C. Boehm, J. Da Silva, P. Richardson and C. Wymant, Phys. Rev. D **86** (2012) 035023 doi:10.1103/PhysRevD.86.035023 [arXiv:1203.3446 [hep-ph]].

[11] G. Belanger, U. Ellwanger, J. F. Gunion, Y. Jiang, S. Kraml and J. H. Schwarz, JHEP **1301** (2013) 069 doi:10.1007/JHEP01(2013)069 [arXiv:1210.1976 [hep-ph]].

[12] S. F. King, M. Mühlleitner, R. Nevzorov and K. Walz, Nucl. Phys. B **870** (2013) 323 doi:10.1016/j.nuclphysb.2013.01.020 [arXiv:1211.5074 [hep-ph]].

[13] M. Badziak, M. Olechowski and S. Pokorski, JHEP **1306** (2013) 043 [arXiv:1304.5437 [hep-ph]].

[14] N. D. Christensen, T. Han, Z. Liu and S. Su, JHEP **1308** (2013) 019 doi:10.1007/JHEP08(2013)019 [arXiv:1303.2113 [hep-ph]].

[15] R. Barbieri, D. Buttazzo, K. Kannike, F. Sala and A. Tesi, Phys. Rev. D **88** (2013) 055011 doi:10.1103/PhysRevD.88.055011 [arXiv:1307.4937 [hep-ph]].

[16] J. Cao, F. Ding, C. Han, J. M. Yang and J. Zhu, JHEP **1311** (2013) 018 doi:10.1007/JHEP11(2013)018 [arXiv:1309.4939 [hep-ph]].

[17] U. Ellwanger and C. Hugonie, JHEP **1408** (2014) 046 doi:10.1007/JHEP08(2014)046 [arXiv:1405.6647 [hep-ph]].

[18] K. Huitu and H. Waltari, JHEP **1411** (2014) 053 doi:10.1007/JHEP11(2014)053 [arXiv:1405.5330 [hep-ph]].

[19] S. F. King, M. Mühlleitner, R. Nevzorov and K. Walz, Phys. Rev. D **90** (2014) 9, 095014 doi:10.1103/PhysRevD.90.095014 [arXiv:1408.1120 [hep-ph]].

[20] K. S. Jeong, Y. Shoji and M. Yamaguchi, JHEP **1411** (2014) 148 doi:10.1007/JHEP11(2014)148 [arXiv:1407.0955 [hep-ph]].

[21] M. Guchait and J. Kumar, arXiv:1509.02452 [hep-ph].

[22] A. Bottino, N. Fornengo and S. Scopel, Phys. Rev. D **85** (2012) 095013 doi:10.1103/PhysRevD.85.095013 [arXiv:1112.5666 [hep-ph]].

[23] C. Boehm, P. S. B. Dev, A. Mazumdar and E. Pukartas, JHEP **1306** (2013) 113 doi:10.1007/JHEP06(2013)113 [arXiv:1303.5386 [hep-ph]].

[24] G. Belanger, G. Drieu La Rochelle, B. Dumont, R. M. Godbole, S. Kraml and S. Kulkarni, Phys. Lett. B **726** (2013) 773 doi:10.1016/j.physletb.2013.09.059 [arXiv:1308.3735 [hep-ph]].

[25] A. Arbey, M. Battaglia and F. Mahmoudi, Phys. Rev. D **88** (2013) 095001 doi:10.1103/PhysRevD.88.095001 [arXiv:1308.2153 [hep-ph]].

[26] J. Cao, C. Han, L. Wu, P. Wu and J. M. Yang, JHEP **1405** (2014) 056 doi:10.1007/JHEP05(2014)056 [arXiv:1311.0678 [hep-ph]].

[27] C. Beskidt, W. de Boer and D. I. Kazakov, Phys. Lett. B **738** (2014) 505 doi:10.1016/j.physletb.2014.08.011 [arXiv:1402.4650 [hep-ph]].

[28] T. Han, Z. Liu and S. Su, JHEP **1408** (2014) 093 doi:10.1007/JHEP08(2014)093 [arXiv:1406.1181 [hep-ph]].

[29] G. D. Kribs, E. Poppitz and N. Weiner, Phys. Rev. D **78** (2008) 055010 [arXiv:0712.2039 [hep-ph]].

[30] A. Salam and J. A. Strathdee, Nucl. Phys. B **87** (1975) 85.

[31] P. Fayet, Nucl. Phys. B **90** (1975) 104.

[32] E. Dudas, M. Goodsell, L. Heurtier and P. Tziveloglou, Nucl. Phys. B **884** (2014) 632 [arXiv:1312.2011 [hep-ph]].

[33] G. D. Kribs and A. Martin, Phys. Rev. D **85** (2012) 115014 [arXiv:1203.4821 [hep-ph]].

[34] G. Belanger, K. Benakli, M. Goodsell, C. Moura and A. Pukhov, JCAP **0908** (2009) 027 [arXiv:0905.1043 [hep-ph]].

[35] E. J. Chun, J. -C. Park and S. Scopel, JCAP **1002** (2010) 015 [arXiv:0911.5273 [hep-ph]].

[36] M. R. Buckley, D. Hooper and J. Kumar, Phys. Rev. D **88** (2013) 063532 [arXiv:1307.3561].

[37] P. J. Fox, A. E. Nelson and N. Weiner, JHEP **0208** (2002) 035 [hep-ph/0206096].

[38] T. Plehn and T. M. P. Tait, J. Phys. G **36** (2009) 075001 [arXiv:0810.3919 [hep-ph]].

[39] S. Y. Choi, M. Drees, J. Kalinowski, J. M. Kim, E. Popenda and P. M. Zerwas, Phys. Lett. B **672** (2009) 246 [arXiv:0812.3586 [hep-ph]].

[40] S. Y. Choi, D. Choudhury, A. Freitas, J. Kalinowski, J. M. Kim and P. M. Zerwas, JHEP **1008** (2010) 025 [arXiv:1005.0818 [hep-ph]].

[41] S. Y. Choi, D. Choudhury, A. Freitas, J. Kalinowski and P. M. Zerwas, Phys. Lett. B **697** (2011) 215 [Erratum-ibid. B **698** (2011) 457] [arXiv:1012.2688 [hep-ph]].

[42] K. Benakli, M. D. Goodsell and F. Staub, JHEP **1306** (2013) 073 [arXiv:1211.0552 [hep-ph]].

[43] G. Aad *et al.* [ATLAS Collaboration], Eur. Phys. J. C **73** (2013) 1, 2263 [arXiv:1210.4826 [hep-ex]].

[44] The ATLAS collaboration [ATLAS Collaboration], ATLAS-CONF-2013-051.

[45] W. Kotlarski, A. Kalinowski and J. Kalinowski, Acta Phys. Polon. B **44** (2013) 11, 2149.

[46] P. Diessner, J. Kalinowski, W. Kotlarski and D. Stöckinger, JHEP **1412** (2014) 124 [arXiv:1410.4791 [hep-ph]].

[47] P. Diessner, J. Kalinowski, W. Kotlarski and D. Stöckinger, Adv. High Energy Phys. **2015** (2015) 760729 doi:10.1155/2015/760729 [arXiv:1504.05386 [hep-ph]].

[48] E. Bertuzzo, C. Frugiuele, T. Gregoire and E. Ponton, JHEP **1504** (2015) 089 [arXiv:1402.5432 [hep-ph]].

[49] S. P. Martin, Phys. Rev. D **92** (2015) 3, 035004 doi:10.1103/PhysRevD.92.035004 [arXiv:1506.02105 [hep-ph]].

[50] Wolfram Research, Inc., Mathematica Version 9.0/10.0, Champaign, IL (2012/2014) .

[51] F. Staub, arXiv:0806.0538 [hep-ph].

[52] F. Staub, Comput. Phys. Commun. **181** (2010) 1077 [arXiv:0909.2863 [hep-ph]].

[53] F. Staub, Comput. Phys. Commun. **182** (2011) 808 [arXiv:1002.0840 [hep-ph]].

[54] F. Staub, Comput. Phys. Commun. **184** (2013) 1792 [arXiv:1207.0906 [hep-ph]].

[55] F. Staub, Comput. Phys. Commun. **185** (2014) 1773 [arXiv:1309.7223 [hep-ph]].

[56] M. D. Goodsell, K. Nickel and F. Staub, Eur. Phys. J. C **75** (2015) 1, 32 [arXiv:1411.0675 [hep-ph]].

[57] W. Porod, Comput. Phys. Commun. **153** (2003) 275 [hep-ph/0301101].

[58] W. Porod and F. Staub, Comput. Phys. Commun. **183** (2012) 2458 [arXiv:1104.1573 [hep-ph]].

[59] P. Athron, J. -h. Park, D. Stöckinger and A. Voigt, arXiv:1406.2319 [hep-ph].

[60] B. C. Allanach, Comput. Phys. Commun. **143** (2002) 305 [hep-ph/0104145].

[61] B. C. Allanach, P. Athron, L. C. Tunstall, A. Voigt and A. G. Williams, Comput. Phys. Commun. **185** (2014) 2322 [arXiv:1311.7659 [hep-ph]].

[62] T. Hahn, Comput. Phys. Commun. **140** (2001) 418 [hep-ph/0012260].

[63] B. Chokoufe Nejad, T. Hahn, J. -N. Lang and E. Mirabella, arXiv:1310.0274 [hep-ph].

[64] T. Hahn and M. Perez-Victoria, Comput. Phys. Commun. **118** (1999) 153 [hep-ph/9807565].

[65] P. Bechtle, O. Brein, S. Heinemeyer, G. Weiglein and K. E. Williams, Comput. Phys. Commun. **181** (2010) 138

[66] P. Bechtle, O. Brein, S. Heinemeyer, G. Weiglein and K. E. Williams, Comput. Phys. Commun. **182** (2011) 2605

[67] P. Bechtle, O. Brein, S. Heinemeyer, O. Stål, T. Stefaniak, G. Weiglein and K. Williams, PoS CHARGED **2012** (2012) 024

[68] P. Bechtle, O. Brein, S. Heinemeyer, O. Stål, T. Stefaniak, G. Weiglein and K. E. Williams, Eur. Phys. J. C **74** (2014) 2693

[69] P. Bechtle, S. Heinemeyer, O. Stål, T. Stefaniak and G. Weiglein, Eur. Phys. J. C **74** (2014) 2711 [arXiv:1305.1933 [hep-ph]].

[70] O. Stål and T. Stefaniak, PoS EPS **-HEP2013** (2013) 314 [arXiv:1310.4039 [hep-ph]].

[71] T. Robens and T. Stefaniak, Eur. Phys. J. C **75** (2015) 104 doi:10.1140/epjc/s10052-015-3323-y [arXiv:1501.02234 [hep-ph]].

[72] F. Domingo and G. Weiglein, arXiv:1509.07283 [hep-ph].

[73] G. Aad *et al.* [ATLAS Collaboration], JHEP **1405** (2014) 071 [arXiv:1403.5294 [hep-ex]].

[74] V. Khachatryan *et al.* [CMS Collaboration], Phys. Rev. D **90** (2014) 9, 092007 [arXiv:1409.3168 [hep-ex]].

[75] G. Aad *et al.* [ATLAS Collaboration], JHEP **1410** (2014) 96 [arXiv:1407.0350 [hep-ex]].

[76] C. Degrande, C. Duhr, B. Fuks, D. Grellscheid, O. Mattelaer and T. Reiter, Comput. Phys. Commun. **183** (2012) 1201 [arXiv:1108.2040 [hep-ph]].

[77] M. Bahr *et al.*, Eur. Phys. J. C **58** (2008) 639 [arXiv:0803.0883 [hep-ph]].

[78] J. Bellm *et al.*, arXiv:1310.6877 [hep-ph].

[79] M. H. Seymour and A. Siodmok, JHEP **1310** (2013) 113 [arXiv:1307.5015 [hep-ph]].

[80] A. Sherstnev and R. S. Thorne, Eur. Phys. J. C **55** (2008) 553 [arXiv:0711.2473 [hep-ph]].

[81] M. Drees, H. Dreiner, D. Schmeier, J. Tattersall and J. S. Kim, Comput. Phys. Commun. **187** (2014) 227 [arXiv:1312.2591 [hep-ph]].

[82] J. de Favereau *et al.* [DELPHES 3 Collaboration], JHEP **1402** (2014) 057 [arXiv:1307.6346 [hep-ex]].

[83] M. Cacciari, G. P. Salam and G. Soyez, Eur. Phys. J. C **72** (2012) 1896 [arXiv:1111.6097 [hep-ph]].

[84] M. Cacciari and G. P. Salam, Phys. Lett. B **641** (2006) 57 [hep-ph/0512210].

[85] M. Cacciari, G. P. Salam and G. Soyez, JHEP **0804** (2008) 063 [arXiv:0802.1189 [hep-ph]].

[86] A. L. Read, J. Phys. G **28** (2002) 2693.

[87] The ATLAS collaboration [ATLAS Collaboration], ATLAS-CONF-2013-049.

[88] [ATLAS Collaboration], ATLAS-CONF-2013-035.

[89] G. Aad *et al.* [ATLAS Collaboration], JHEP **1404** (2014) 169 [arXiv:1402.7029 [hep-ex]].

[90] [ATLAS Collaboration], ATLAS-CONF-2013-036.

[91] J. Alwall *et al.*, JHEP **1407** (2014) 079 [arXiv:1405.0301 [hep-ph]].

[92] A. Belyaev, N. D. Christensen and A. Pukhov, Comput. Phys. Commun. **184** (2013) 1729 [arXiv:1207.6082 [hep-ph]].

[93] G. Aad *et al.* [ATLAS Collaboration], Eur. Phys. J. C **75** (2015) 5, 208 [arXiv:1501.07110 [hep-ex]].

[94] G. Belanger, F. Boudjema, A. Pukhov and A. Semenov, Comput. Phys. Commun. **192** (2015) 322 [arXiv:1407.6129 [hep-ph]].

[95] C. Savage, A. Scaffidi, M. White and A. G. Williams, arXiv:1502.02667 [hep-ph].

[96] D. S. Akerib *et al.* [LUX Collaboration], Nucl. Instrum. Meth. A **704** (2013) 111 [arXiv:1211.3788 [physics.ins-det]].

[97] K. A. Olive *et al.* [Particle Data Group Collaboration], Chin. Phys. C **38** (2014) 090001.

[98] P. A. R. Ade *et al.* [Planck Collaboration], Astron. Astrophys. **571** (2014) A16 [arXiv:1303.5076 [astro-ph.CO]].